Beam Tracking Based on Variable Step Beam for Millimeter Wave Massive MIMO

Zhenjiang Xiao, *Student Member, IEEE*, Chenhao Qi, *Senior Member, IEEE*, and Juan Nie

***Abstract*— In this letter, a beam tracking scheme based on variable step beam (VSB) is proposed for millimeter wave (mmWave) massive MIMO. Firstly, a design method for VSB is proposed, where a small portion of the beam energy is taken to track the movement of user equipment (UE) and the large portion of the beam energy is used to keep the quality of current mmWave communication link. Then based on the beam sweeping using VSBs, the angle-of-departure (AoD) of the UE is estimated by iteratively updating the posterior probability together with the range prediction of the fading coefficient of the mmWave channel, where the mainlobe of the VSBs is iteratively updated by Gaussian process regression to cover the movement of the UE. Simulation results verify the effectiveness of the proposed scheme and show that it has larger achievable rate than the existing schemes.**

***Index Terms*— Angle-of-departure (AoD) estimation, beam tracking, millimeter wave (mmWave) communications, step beam.**

I. Introduction

MILLIMETER wave (mmWave) communications can provide high data rate wireless transmission by directional beamforming. But on the other side, the mobility of the user equipment (UE) brings a big challenge for mmWave mobile communications. To achieve beam alignment to the mmWave massive MIMO channel between the transmitter and the receiver, beam training is typically adopted, where the basic method is the beam sweeping [1]. However, the training overhead is not negligible for beam training. To benefit from the channel coherence for the reduction of the training overhead, beam tracking is adopted. Different from the beam sweeping that makes a completely new probing of the spatial region, the beam tracking only probes a small spatial region of interest based on the previous information with low overhead.

The existing beam tracking methods for mmWave massive MIMO can be divided into two categories, including classic methods and machine learning (ML)-based methods. For the first category, a low-overhead beam sweeping is used to probe the neighborhood of the current beam, i.e., neighborhood beam sweeping (NBS), where a variable-length frame structure is employed for better adaption to the UE's movement [2]. Similar to the motivation of Sub-6GHz MIMO channel tracking, Kalman filtering and particle filtering are used for beam tracking for mmWave massive MIMO [3], [4]. For the second category, a recurrent neural network with a modified cost function is used to track the angle of the mobile UE [5]. In [6] and [7], the angle of the mobile UE is modeled as a stochastic process, where Gaussian process regression (GPR) is adopted to predict the angle of UE. Compared to [6], the update of beam coverage is further considered to ensure that the beam covers the movement of the UE [7].

In this letter, we propose a beam tracking scheme based on variable step beam (VSB). Firstly, the design method for VSB is proposed, where a small portion of the beam energy is taken to track the UE's movement and the large portion of the beam energy is used to keep the quality of current mmWave communication link. Then based on the beam sweeping using VSBs, the angle-of-departure (AoD) of the UE is estimated by iteratively updating the posterior probability together with the range prediction of the fading coefficient of the mmWave channel, where the mainlobe of the VSBs is iteratively updated by GPR to cover the movement of the UE.

Notations: Symbols for vectors (lower case) and matrices (upper case) are in boldface. $(\cdot)^{\mathrm{T}}$, $(\cdot)^{\mathrm{H}}$, $|\cdot|$ and $\|\cdot\|_2$ denote the transpose, the conjugate transpose, the absolute value and the l_2-norm, respectively. $[\boldsymbol{a}]_m$ represents the mth element of the vector $\boldsymbol{a}$ and $[\boldsymbol{A}]_{m,n}$ represents the entry located in the mth row and nth column of the matrix $\boldsymbol{A}$. $\mathcal{CN}(\mu, \sigma^2)$ denotes the complex Gaussian distribution with the mean being μ and the variance being σ^2. Symbol $\mathbb{C}$ and $\mathbb{Z}$ denote the sets of complex-valued numbers and integers, respectively.

II. System Model

We consider a mmWave massive MIMO system including a base station (BS) and a single-antenna UE, where the BS is equipped with a uniform linear array (ULA) composed of N_{BS} antennas. According to the widely used Saleh-Valenzuela channel model [8], the channel vector at the tth time slot between the BS and the UE can be expressed as

$$\boldsymbol{h}(t) = \sqrt{\frac{N_{\mathrm{BS}}}{L(t)}} \sum_{l=1}^{L(t)} \alpha_l(t) \boldsymbol{a}^{\mathrm{H}}\big(N_{\mathrm{BS}}, \phi_l(t)\big), \quad t \in \mathbb{Z}, \tag{1}$$

where $L(t)$, $\alpha_l(t)$ and $\phi_l(t)$ denote the number of channel paths, the complex-valued fading coefficient and the AoD of the lth channel path, respectively. The channel steering vector $\boldsymbol{a}(N_{\mathrm{BS}}, \phi)$ as a function of N_{BS} and ϕ is defined as

$$\boldsymbol{a}(N_{\mathrm{BS}}, \phi) \triangleq \frac{1}{\sqrt{N_{\mathrm{BS}}}} \left[1, e^{j\frac{2\pi d}{\lambda}\phi}, \ldots, e^{j\frac{2\pi d}{\lambda}(N_{\mathrm{BS}}-1)\phi}\right]^{\mathrm{T}}, \tag{2}$$

where λ denotes the signal wavelength, d denotes the distance of two adjacent antenna elements of the ULA and ϕ is the channel AoD. Typically we set $d = \lambda/2$.

During the downlink signal transmission from the BS to the UE, the received signal at the tth time slot is

$$y(t) = \sqrt{P}\boldsymbol{h}(t)\boldsymbol{f}(t)s(t) + \eta(t), \tag{3}$$

Manuscript received 25 June 2023; accepted 16 July 2023. Date of publication 19 July 2023; date of current version 12 September 2023. This work is supported in part by National Natural Science Foundation of China under Grant 62071116. The associate editor coordinating the review of this letter and approving it for publication was Q. Wu. *(Corresponding author: Chenhao Qi.)*

The authors are with the School of Information Science and Engineering, Southeast University, Nanjing 210096, China (e-mail: 220220826@seu.edu.cn; qch@seu.edu.cn; 220200798@seu.edu.cn).

Digital Object Identifier 10.1109/LCOMM.2023.3296723

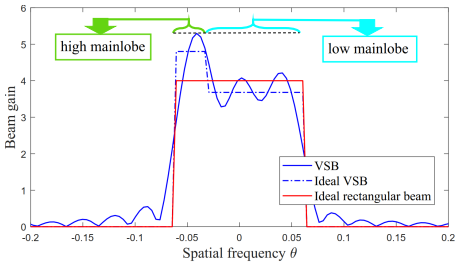

Fig. 1. Illustration of the variable step beam.

where P denotes the transmit power of the BS, $s(t)$ with $|s(t)|^2 = 1$ denotes the data symbol, $\boldsymbol{f}(t) \in \mathbb{C}^{N_{\mathrm{BS}}}$ with $\|\boldsymbol{f}(t)\|_2^2 = 1$ denotes the beamforming vector of the BS and $\eta(t) \backsim \mathcal{CN}(0, \sigma_\eta^2)$ denotes the additive white Gaussian noise at the tth time slot.

The transmission signal is in unit of frames, where the length of each frame is T_{f} and each frame contains L_{f} time slots. Therefore, the length of each time slot is $T_{\mathrm{s}} = T_{\mathrm{f}}/L_{\mathrm{f}}$. Each frame is consist of a beam sweeping unit or a beam tracking unit and a data transmission unit. After finishing the data transmission, the UE feeds back the received signal power to the BS, i.e., reference signal receiving power (RSRP). If the RSRP is under a predefined threshold, the beam sweeping unit will be used; otherwise, the beam tracking unit will be used. Note that different from the beam sweeping that makes a completely new probing of the spatial region, the beam tracking only probes a small spatial region of interest based on the AoD of the previous frame with low overhead.

III. Beam Tracking Based on VSB

A. VSB Design

As shown in Fig. 1, we propose a VSB, where the mainlobe of the VSB points at the UE for mmWave communications. As a comparison, we also show the ideal rectangular beam that can clearly indicate the mainlobe. Due to the UE's mobility, the UE may move from the center to the edge of the mainlobe. Therefore, we need to use beam tracking to follow the UE's movement. To avoid the communication interruption, we do not want to change the direction or the width of the current beam. Instead, we may consider to change the beam gain of the mainlobe of the beam. Note that the large-scale antenna array offers a high degree of freedom for beam design, which makes that the variable beam gain within the mainlobe can be easily implemented. As shown in Fig. 1, the high mainlobe of the VSB points at the spatial direction that the UE may move in. Compared to the ideal rectangular beam, the VSB increases the beam gain of high mainlobe by reducing the beam gain of low mainlobe, where the power of the VSB is the same as that of the ideal rectangular beam. In this way, we can generate different VSBs that have different positions of high mainlobe, and then use these VSBs to track the movement of the UE.

We divide the mainlobe of the beam into S narrower spatial regions, where each spatial region is covered by the high mainlobe of a VSB. To fast generate these VSBs, we define a codebook $\boldsymbol{\mathcal{F}} \triangleq [\boldsymbol{f}_1, \boldsymbol{f}_2, \ldots, \boldsymbol{f}_S]$. The beam gain of the sth VSB $\boldsymbol{f}_s$, for $s = 1, 2, \ldots, S$, can be expressed as

$$G(\boldsymbol{f}_s, \theta) \triangleq \begin{cases} C_{\mathrm{l}}, & \theta \in [-\frac{B}{2} + \theta_{\mathrm{c}}, \frac{B}{2} + \theta_{\mathrm{c}}], \\ & \text{and } \theta \notin [\theta_{\mathrm{h}} - \frac{B}{2S}, \theta_{\mathrm{h}} + \frac{B}{2S}], \\ C_{\mathrm{h}}, & \theta \in [\theta_{\mathrm{h}} - \frac{B}{2S}, \theta_{\mathrm{h}} + \frac{B}{2S}], \\ 0, & \text{otherwise}, \end{cases} \tag{4}$$

where B and θ_{c} denote the width and the center angle of the mainlobe, respectively, and $\theta_{\mathrm{h}} \triangleq \theta_{\mathrm{c}} - B/2 + (2s-1)B/2S$ is the center angle of the high mainlobe of the sth VSB. Moreover, we define

$$C_{\mathrm{l}} \triangleq \sqrt{2(1-\gamma)/B}, \tag{5}$$

$$C_{\mathrm{h}} \triangleq \sqrt{2\big(1+\gamma(S-1)\big)/B}, \tag{6}$$

where γ is a factor to determine C_{l} and C_{h}. To maintain the current link of mmWave communications, we need to set C_{l} enough large so that the communication quality of the UE is guaranteed. As shown in Fig. 1, we give an example of a VSB that is designed based on the schemes [9] with $N_{\mathrm{BS}} = 64$, $S = 4$, $s = 1$, $\theta_{\mathrm{c}} = 0$, $B = 8/N_{\mathrm{BS}}$ and $\gamma = 0.15$.

In fact, the motivation of the VSB is to take a small portion of the energy of the beam to track the UE movement, while the large portion of the energy of the beam is used to keep the quality of current mmWave communication link. The VSB will be mostly used by the scenario that the communication quality is of satisfactory, considering that the UE's movement without effective beam tracking will lead to severe communication interruption. Note that different from the existing works that additional resource is needed for beam tracking to maintain current communication link, the VSB can maintain current communication link and perform beam tracking simultaneously, which does not need additional resource such as additional beam.

B. AoD Estimation

Based on $\boldsymbol{\mathcal{F}}$, the BS can perform the beam sweeping to probe the spatial regions of the mainlobe by transmitting S VSBs. Based on the results of beam sweeping, we can determine the AoD of the UE by selecting θ_{h} of the VSB resulting the largest RSRP, where the resolution of the AoD estimation is B/S. Moreover, the difference of the beam gain between the high mainlobe and the low mainlobe may not be large enough to get satisfactory beam sweeping results with highly differentiated RSRP.

Inspired by [10], we may use the channel model (1), the noise distribution $\mathcal{CN}(0, \sigma_\eta^2)$ and beam sweeping based on $\boldsymbol{\mathcal{F}}$, to estimate the AoD. Since the fading coefficient of the non-LOS (NLOS) path is much weaker than that of the LOS path [1], we consider the AoD estimation of the LOS path. To simplify the notation, we redefine the fading coefficient of the LOS path in (1) as $\alpha(t) \triangleq \alpha_1(t)$. Note that $\alpha(t)$ is assumed to be a constant within each frame. We define $n \triangleq \lceil t/L_{\mathrm{f}} \rceil$ to be the index of the frame, so that $\alpha(n)$ denotes the fading coefficient of the LOS path of the nth frame, for $n = 1, 2, \ldots, N$, where N denotes the number of frames for beam tracking.

We quantize the AoD in $[-1,1]$, where the angle resolution is set as $2/Q$ with $Q \geq N_{\mathrm{BS}}$. Then the set of the quantized angles can be defined as $\Theta \triangleq \{\theta_1, \theta_2, \ldots, \theta_Q\}$, where $\theta_i \triangleq -1 + (2i-1)/Q$ for $i = 1, 2, \ldots, Q$. We denote t_s as the index of the time slot when $\boldsymbol{f}_s$ is used for beam sweeping, i.e., $\boldsymbol{f}(t_s) = \boldsymbol{f}_s$. Given the received signals and the transmit beams in the previous s time slots, the posterior probability at the t_sth time slot is defined as $\boldsymbol{\pi}(t_s) \in \mathbb{C}^Q$, whose ith element is expressed as

$$[\boldsymbol{\pi}(t_s)]_i \triangleq \mathbb{P}\big(\phi = \theta_i | y(t_1), y(t_2), \ldots, y(t_s), \boldsymbol{f}(t_1), \boldsymbol{f}(t_2), \ldots, \boldsymbol{f}(t_s)\big). \tag{7}$$

According to Bayes theorem, the posterior probability can be updated as

$$[\boldsymbol{\pi}(t_{s+1})]_i = \frac{[\boldsymbol{\pi}(t_s)]_i \mathbb{P}\big(y(t_{s+1}) | \phi = \theta_i, \boldsymbol{f}(t_{s+1})\big)}{\sum_{q=1}^{Q} [\boldsymbol{\pi}(t_s)]_q \mathbb{P}\big(y(t_{s+1}) | \phi = \theta_q, \boldsymbol{f}(t_{s+1})\big)}. \tag{8}$$

For simplicity, we can rewrite (3) as $y(t) \approx \alpha(n) g_i(t) + \eta(t)$, where $g_i(t) \triangleq \sqrt{P N_{\mathrm{BS}}/L(t)} \boldsymbol{a}^{\mathrm{H}}(N_{\mathrm{BS}}, \theta_i) \boldsymbol{f}(t)$. And the conditional probability in (8) can expressed as

$$\mathbb{P}\big(y(t) | \phi = \theta_i, \boldsymbol{f}(t)\big) = \frac{1}{\sqrt{2\pi}\sigma_\eta} e^{-\frac{|y(t) - \alpha(n) g_i(t)|^2}{2\sigma_\eta^2}}. \tag{9}$$

According to [10], an accurate estimate of the fading coefficient $\hat{\alpha}(n)$ is required to update the posterior probability. However, for mmWave mobile communications, the fading coefficient is difficult to be accurately estimated.

Different from [10], in this letter we do not rely on an accurate estimate of the fading coefficient. Since $\alpha(n)$ and $\eta(t_s)$ are independent to each other, the conditional probability in (9) can be derived as

$$\begin{aligned} &\mathbb{P}\big(y(t) | \phi = \theta_i, \boldsymbol{f}(t)\big) \\ &\approx \int_{-\infty}^{\infty} \mathbb{P}_\alpha\big(y(t) - \eta(t) | \phi = \theta_i, \boldsymbol{f}(t)\big) \mathbb{P}_\eta\big(\eta(t)\big)\, \mathrm{d}\eta(t) \\ &= -\int_{-\infty}^{\infty} \mathbb{P}_\alpha\big(\alpha(n) | \theta_i, \boldsymbol{f}(t)\big) \mathbb{P}_\eta\big(y(t) - \alpha(n) g_i(t)\big)\, \mathrm{d}\alpha(n) \end{aligned} \tag{10}$$

where

$$\mathbb{P}_\eta\big(y(t) - \alpha(n) g_i(t)\big) = \frac{1}{\sqrt{2\pi}\sigma_\eta} e^{-\frac{|y(t) - \alpha(n) g_i(t)|^2}{2\sigma_\eta^2}}. \tag{11}$$

Since the integration in (10) is difficult to be computed, we resort to approximate the integration in (10) by quantizing $\alpha(n)$. To represent the range of $\alpha(n)$, we denote the maximum and the minimum of the real part of $\alpha(n)$ as $r_{\max}(n)$ and $r_{\min}(n)$, respectively, and then quantize the real part of $\alpha(n)$ into δ_{r} equal intervals, where the mth interval can be denoted as

$$r_m(n) = r_{\min}(n) + (m-1)\big(r_{\max}(n) - r_{\min}(n)\big)/\delta_{\mathrm{r}}, \tag{12}$$

for $m = 1, 2, \ldots, \delta_{\mathrm{r}}$. Similarly, we denote the maximum and the minimum of the imaginary part of $\alpha(n)$ as $z_{\max}(n)$ and $z_{\min}(n)$, respectively, and then quantize the imaginary part of $\alpha(n)$ into δ_{z} equal intervals, where the kth interval can be denoted as

$$z_k(n) = z_{\min}(n) + (k-1)\big(z_{\max}(n) - z_{\min}(n)\big)/\delta_{\mathrm{z}}, \tag{13}$$

for $k = 1, 2, \ldots, \delta_{\mathrm{z}}$. In fact, the integration on $\alpha(n)$ can be divided into the separate integration on the real part of $\alpha(n)$ and on the imaginary part of $\alpha(n)$, i.e., $\mathrm{d}\alpha(n) = \mathrm{dRe}\{\alpha(n)\}\mathrm{dIm}\{\alpha(n)\}$. Then we can approximately compute (10) and then substitute it into (8) to obtain (14), as shown at the bottom of the page.

Since $[\boldsymbol{\pi}(t_{s+1})]_i$ in (14) is independent of $\alpha(n)$, in order to estimate $\alpha(n)$, we define

$$[\widetilde{\boldsymbol{\pi}}(t_s)]_{i,m,k} \triangleq \mathbb{P}_\alpha\big(r_m(n), z_k(n) | \theta_i, \boldsymbol{f}(t_{s+1})\big) [\boldsymbol{\pi}(t_s)]_i. \tag{15}$$

According to (14), the posterior probability is updated by

$$\begin{aligned} &[\widetilde{\boldsymbol{\pi}}(t_{s+1})]_{i,m,k} \\ &= \sum_{m'=1}^{\delta_{\mathrm{r}}} \sum_{k'=1}^{\delta_{\mathrm{z}}} \sum_{q'=1}^{Q} \\ &\frac{\mathbb{P}_\eta\big(y(t_{s+1}) - \big(r_m(n) + j z_k(n)\big) g_i(t_{s+1})\big) [\widetilde{\boldsymbol{\pi}}(t_s)]_{i,m,k}}{\mathbb{P}_\eta\big(y(t_{s+1}) - \big(r_{m'}(n) + j z_{k'}(n)\big) g_{q'}(t_{s+1})\big) [\widetilde{\boldsymbol{\pi}}(t_s)]_{q',m',k'}}. \end{aligned} \tag{16}$$

To initialize the posterior probability in (15), we denote the indices of the quantized lower bound and upper bound of the mainlobe in Θ as i_{l} and i_{u}, respectively. Then we can initialize the posterior probability in (15) by

$$[\widetilde{\boldsymbol{\pi}}(t_0)]_{i,m,k} = \frac{1}{(i_{\mathrm{u}} - i_{\mathrm{l}} + 1)\delta_{\mathrm{r}}\delta_{\mathrm{z}}}, \tag{17}$$

for $i = i_{\mathrm{l}}, i_{\mathrm{l}}+1, \ldots, i_{\mathrm{u}}$, $m = 1, 2, \ldots, \delta_{\mathrm{r}}$ and $k = 1, 2, \ldots, \delta_{\mathrm{z}}$. Based on (15), the posterior probabilities of the estimation of the AoD, the real part and imaginary part of fading coefficient are expressed respectively as

$$\begin{aligned} [\boldsymbol{\pi}(t_s)]_i &= \sum_{m=1}^{\delta_{\mathrm{r}}} \sum_{k=1}^{\delta_{\mathrm{z}}} [\widetilde{\boldsymbol{\pi}}(t_s)]_{i,m,k}, \quad i = 1, 2, \ldots, Q, \\ [\boldsymbol{\Omega}(t_s)]_m &= \sum_{i=1}^{Q} \sum_{k=1}^{\delta_{\mathrm{z}}} [\widetilde{\boldsymbol{\pi}}(t_s)]_{i,m,k}, \quad m = 1, 2, \ldots, \delta_{\mathrm{r}}, \\ [\boldsymbol{\Lambda}(t_s)]_k &= \sum_{i=1}^{Q} \sum_{m=1}^{\delta_{\mathrm{r}}} [\widetilde{\boldsymbol{\pi}}(t_s)]_{i,m,k}, \quad k = 1, 2, \ldots, \delta_{\mathrm{z}}. \end{aligned} \tag{18}$$

After finishing S iterations, we can determine the AoD for the nth frame by $\hat{\phi}(n) = \hat{\phi}(t_S)$, which will be used by the next subsection. The indices of the estimated AoD, the real

$$\begin{aligned} [\boldsymbol{\pi}(t_{s+1})]_i &= \frac{\sum_{m=1}^{\delta_r} \sum_{k=1}^{\delta_z} \mathbb{P}_\eta\big(y(t_{s+1}) - \big(r_m(n) + j z_k(n)\big) g_i(t_{s+1})\big) \mathbb{P}_\alpha\big(r_m(n), z_k(n) | \theta_i, \boldsymbol{f}(t_{s+1})\big) \delta_r \delta_z [\boldsymbol{\pi}(t_s)]_i}{\sum_{m'=1}^{\delta_r} \sum_{k'=1}^{\delta_z} \sum_{q'=1}^{Q} \mathbb{P}_\eta\big(y(t_{s+1}) - \big(r_{m'}(n) + j z_{k'}(n)\big) g_{q'}(t_{s+1})\big) \mathbb{P}_\alpha\big(r_{m'}(n), z_{k'}(n) | \theta_{q'}, \boldsymbol{f}(t_{s+1})\big) \delta_r \delta_z [\boldsymbol{\pi}(t_s)]_{q'}} \\ &= \frac{\sum_{m=1}^{\delta_r} \sum_{k=1}^{\delta_z} \mathbb{P}_\eta\big(y(t_{s+1}) - \big(r_m(n) + j z_k(n)\big) g_i(t_{s+1})\big) \mathbb{P}_\alpha\big(r_m(n), z_k(n) | \theta_i, \boldsymbol{f}(t_{s+1})\big) [\boldsymbol{\pi}(t_s)]_i}{\sum_{m'=1}^{\delta_r} \sum_{k'=1}^{\delta_z} \sum_{q'=1}^{Q} \mathbb{P}_\eta\big(y(t_{s+1}) - \big(r_{m'}(n) + j z_{k'}(n)\big) g_{q'}(t_{s+1})\big) \mathbb{P}_\alpha\big(r_{m'}(n), z_{k'}(n) | \theta_{q'}, \boldsymbol{f}(t_{s+1})\big) [\boldsymbol{\pi}(t_s)]_{q'}}. \end{aligned} \tag{14}$$

part and imaginary part of fading coefficient are expressed respectively as

$$\hat{i} = \arg \max_{i=1,2,\ldots,Q} [\boldsymbol{\pi}(t_S)]_i,$$
$$\hat{m} = \arg \max_{m=1,2,\ldots,\delta_\mathrm{r}} [\boldsymbol{\Omega}(t_S)]_m,$$
$$\hat{k} = \arg \max_{k=1,2,\ldots,\delta_\mathrm{z}} [\boldsymbol{\Lambda}(t_S)]_k. \tag{19}$$

Therefore, based on (12) and (13), the estimated fading coefficient for the nth frame is

$$\hat{\alpha}(n) = r_{\hat{m}}(n) + j z_{\hat{k}}(n). \tag{20}$$

The estimated AoD for the t_Sth time slot is

$$\hat{\phi}(t_S) = \theta_{\hat{i}}. \tag{21}$$

Since a range of the fading coefficient $\alpha(n)$ is needed for the quantization so that the integration can be approximated by the summation in (10), we use the GPR model for the prediction of the range of $\alpha(n)$. We define $\boldsymbol{w}(n) \triangleq [\mathrm{Re}\{\hat{\alpha}(n)\}, \mathrm{Im}\{\hat{\alpha}(n)\}]^\mathrm{T}$, where $\hat{\alpha}(n)$ is an estimate of $\alpha(n)$. We establish two data sets as

$$\boldsymbol{X}(n) = [\boldsymbol{w}(n-M-1), \boldsymbol{w}(n-M), \ldots, \boldsymbol{w}(n-2)]^\mathrm{T},$$
$$\boldsymbol{Y}(n) = [\boldsymbol{w}(n-M), \boldsymbol{w}(n-M+1), \ldots, \boldsymbol{w}(n-1)]^\mathrm{T}, \tag{22}$$

where M denotes the length of each data set. Based on the data sets in (22), we can use the GPR model to predict the range of $\alpha(n)$ as

$$r_{\min}(n) = [\boldsymbol{\mu}_\mathrm{w}]_1 - 2[\boldsymbol{\sigma}_\mathrm{w}]_1, r_{\max}(n) = [\boldsymbol{\mu}_\mathrm{w}]_1 + 2[\boldsymbol{\sigma}_\mathrm{w}]_1,$$
$$z_{\min}(n) = [\boldsymbol{\mu}_\mathrm{w}]_2 - 2[\boldsymbol{\sigma}_\mathrm{w}]_2, z_{\max}(n) = [\boldsymbol{\mu}_\mathrm{w}]_2 + 2[\boldsymbol{\sigma}_\mathrm{w}]_2, \tag{23}$$

where $\boldsymbol{\mu}_\mathrm{w}$ and $\boldsymbol{\sigma}_\mathrm{w}$ are the mean and standard deviation of $\boldsymbol{w}(n)$, respectively.

C. Mainlobe Update for VSB

Similar to the range prediction of the fading coefficient in the previous subsection, we can predict the range of the AoD at the $(n+1)$th frame by the GPR model to update the mainlobe of the VSB. Suppose the predicted range of $\hat{\phi}(n+1)$ is $[\mu_\phi - 2\sigma_\phi, \mu_\phi + 2\sigma_\phi]$, where μ_ϕ and σ_ϕ are the mean and standard deviation of $\hat{\phi}(n+1)$, respectively. To ensure that the mainlobe of the VSB covers the movement of the UE at the nth frame while the mainlobe can be as narrow as possible, we can update B and θ_c respectively by

$$B = \begin{cases} 4\sigma_\phi + \dfrac{2}{N_\mathrm{BS}}, & \hat{\phi}(n) \in [\mu_\phi - 2\sigma_\phi, \mu_\phi + 2\sigma_\phi], \\ |\mu_\phi - \hat{\phi}(n)| + 2\sigma_\phi + \dfrac{2}{N_\mathrm{BS}}, & \text{otherwise}. \end{cases}$$
$$\theta_\mathrm{c} = \begin{cases} \mu_\phi, & \hat{\phi}(n) \in [\mu_\phi - 2\sigma_\phi, \mu_\phi + 2\sigma_\phi], \\ \dfrac{\mu_\phi + \hat{\phi}(n) + 2\sigma_\phi}{2}, & \hat{\phi}(n) \in [-1, \mu_\phi - 2\sigma_\phi), \\ \dfrac{\mu_\phi + \hat{\phi}(n) - 2\sigma_\phi}{2}, & \hat{\phi}(n) \in (\mu_\phi + 2\sigma_\phi, 1]. \end{cases} \tag{24}$$

Considering the estimation error, in (24) we add an error-tolerant range of $1/N_\mathrm{BS}$ at both the left and the right of the mainlobe of the VSB.

The procedure of the proposed beam tracking scheme based on VSB is summarized in **Algorithm 1**.

Algorithm 1 Beam Tracking Scheme Based on VSB

Input: B, θ_c, δ_r, δ_z, Q, M and N.

for $n = 1$ **to** N **do**
  if RSRP $>$ threshold **then**
    Establish two data sets via (22).
    Predict the range of the fading coefficient via (23).
    Quantize the predicted range via (12) and (13).
    Update the VSB codebook $\boldsymbol{\mathcal{F}}$ based on B and θ_c.
    Transmit VSBs in $\boldsymbol{\mathcal{F}}$ to obtain $y(t_1), \ldots, y(t_S)$.
    Compute $\widetilde{\boldsymbol{\pi}}(t_0)$ via (17).
    for $s = 1$ **to** S **do**
      Update $\widetilde{\boldsymbol{\pi}}(t_s)$ via (16).
    end for
    Compute $\boldsymbol{\pi}(t_S)$, $\boldsymbol{\Omega}(t_S)$ and $\boldsymbol{\Lambda}(t_S)$ via (18).
    Determine $\hat{\alpha}(n)$ via (20) and $\hat{\phi}(t_S)$ via (21).
    Update B and θ_c via (24).
  else
    Switch to the beam sweeping unit.
  end if
  Start the data transmission.
end for

IV. Simulation Results

Now we evaluate the performance of the proposed scheme. The BS is equipped with $N_\mathrm{BS} = 64$ antennas in ULA, which is positioned along the y-axis with the center at the origin. The single-antenna UE is located at $\big(x_\mathrm{u}(0), y_\mathrm{u}(0)\big) = (5\mathrm{m}, -20\mathrm{m})$ at the initial time slot, and moves in a straight line in the direction $\vartheta = 1.4708$ with velocity $v = 30$m/s, where ϑ is the angle in unit of radian between the direction of velocity and the x-axis. The AoD with time slot t is expressed as

$$\phi(t) = \sin\Big(\arctan\big(y_\mathrm{u}(t)/x_\mathrm{u}(t)\big)\Big) \tag{25}$$

where $x_\mathrm{u}(t) = x_\mathrm{u}(0) + vt\cos\vartheta$ and $y_\mathrm{u}(t) = y_\mathrm{u}(0) + vt\sin\vartheta$ denote the position of the UE.

We set $T_\mathrm{f} = 10$ms, $T_\mathrm{s} = 1/16$ms, $Q = 512$, $\delta_\mathrm{r} = \delta_\mathrm{z} = 50$, $M = 10$, $\gamma = 0.1$ and $S = 4$. We model the time varying fading coefficient as a first-order Markov process, i.e., $\alpha(n+1) = \rho\alpha(n) + \zeta(n)$, where ρ is the correlation coefficient and $\zeta(n) \backsim \mathcal{CN}(0, 1-\rho^2)$. We set $\rho = 0.995$ and initialize $\alpha(1) \backsim \mathcal{CN}(0, 1)$.

We will compare the following five beam tracking schemes: 1) The proposed VSB-based beam tracking scheme, where the fading coefficient is unknown and needs to be predicted by the GPR. 2) The proposed VSB-based beam tracking scheme if the fading coefficient is ideally known. 3) The robust Kalman filtering (RKF) scheme [3]. 4) The neighborhood beam sweeping (NBS) scheme that performs a small-scale beam sweeping only in the neighborhood of θ_c as $[\theta_\mathrm{c} - 3/N_\mathrm{BS}, \theta_\mathrm{c} + 3/N_\mathrm{BS}]$, where the mainlobe width for beam sweeping is $2/N_\mathrm{BS}$. 5) The GPR-based scheme, where the difference between this scheme and the NBS scheme is that the neighborhood of θ_c in the latter is fixed but it is adaptively predicted by the GPR

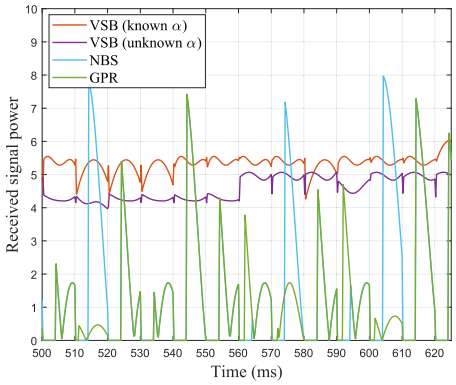

Fig. 2. Comparisons of UE's received signal power in terms of time for different schemes.

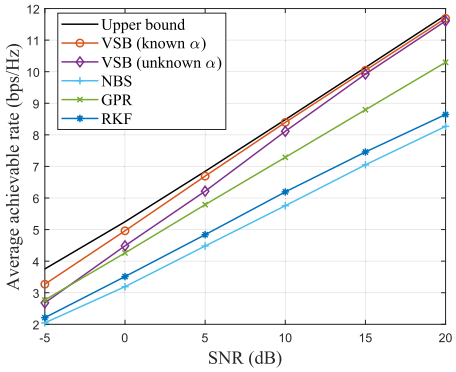

Fig. 3. Comparisons of average achievable rate in terms of SNR for different schemes.

in the former. To show the upper bound for different beam tracking schemes, the performance where the AoD is ideally known is also provided.

Fig. 2 compares the received signal power of the UE in terms of time for different schemes. It is seen that VSB with either ideally known α or unknown α outperforms NBS and GPR by achieving more stable received signal power without severe signal power reduction. In particular, VSB with ideally known α is better than that with unknown α, where we need to predict the range of α based on GPR in our proposed scheme. Due to the mobility of the UE, the UE may move outside of the neighborhood of θ_{c}, which leads to the severe signal power reduction for NBS and GPR. At some time points, NBS or GPR can even outperform VSB, since both NBS and GPR use narrower beam than VSB and can achieve larger beam gain.

Fig. 3 compares the average achievable rate in terms of SNR for different schemes. It is seen that VSB with either ideally known α or unknown α can approach the upper bound as SNR increases. When SNR is higher than 10dB, the achievable rate of VSB with either ideally known α or unknown α can reach 95% of the upper bound. At low SNR, e.g., 0dB or even smaller, the AoD estimation based on iterative posterior probability updating is affected by the noise, which results in a small gap between VSB with ideally known α and the upper bound. Since the prediction of α is also affected by the noise and will further affect the AoD estimation, there is a gap between VSB with ideally known α and VSB with unknown α. Since the neighborhood of θ_{c} is adaptively predicted for GPR but is fixed for NBS, GPR performs much better than NBS. Moreover, both GPR and RKF outperform NBS, because that the AoD prediction is employed by the former two but is not employed by NBS. In particular, GPR is much better than RKF, since M frames are used for GPR but only one frame is used by RKF for the AoD prediction, where GPR can achieve better AoD prediction performance than RKF.

V. Conclusion

In this letter, a beam tracking scheme based on VSB has been proposed for mmWave mobile communications. Based on the beam sweeping using VSBs, UE's AoD has been estimated by iteratively updating the posterior probability together with the range prediction of the fading coefficient of the mmWave channel, where the mainlobe of the VSBs is iteratively updated by GPR to cover the movement of the UE. The future work will be continued by considering the extension of this work to the reconfigurable intelligent surface-assisted mmWave communications for high-precision AoD estimation.

References

[1] C. Qi, P. Dong, W. Ma, H. Zhang, Z. Zhang, and G. Y. Li, "Acquisition of channel state information for mmWave massive MIMO: Traditional and machine learning-based approaches," *Sci. China Inf. Sci.*, vol. 64, no. 8, Aug. 2021, Art. no. 181301.

[2] C. Liu et al., "Robust adaptive beam tracking for mobile millimetre wave communications," *IEEE Trans. Wireless Commun.*, vol. 20, no. 3, pp. 1918–1934, Mar. 2021.

[3] V. Va, H. Vikalo, and R. W. Heath Jr., "Beam tracking for mobile millimeter wave communication systems," in *Proc. IEEE Global Conf. Signal Inf. Process. (GlobalSIP)*, Washington, DC, USA, Dec. 2016, pp. 743–747.

[4] S. Lee, E. S. Lohan, and S. Kim, "Array-based GNSS signal tracking with a reduced state signal model," *IEEE Trans. Aerosp. Electron. Syst.*, vol. 52, no. 3, pp. 1267–1283, Jun. 2016.

[5] D. Burghal, N. A. Abbasi, and A. F. Molisch, "A machine learning solution for beam tracking in mmWave systems," in *Proc. 53rd Asilomar Conf. Signals, Syst., Comput.*, Pacific Grove, CA, USA, Nov. 2019, pp. 173–177.

[6] J. Zhang, C. Masouros, and Y. Huang, "Beam training and tracking with limited sampling sets: Exploiting environment priors," *IEEE Trans. Commun.*, vol. 71, no. 5, pp. 3008–3023, May 2023.

[7] H.-L. Song and Y.-C. Ko, "Beam alignment for high-speed UAV via angle prediction and adaptive beam coverage," *IEEE Trans. Veh. Technol.*, vol. 70, no. 10, pp. 10185–10192, Oct. 2021.

[8] X. Sun, C. Qi, and G. Y. Li, "Beam training and allocation for multiuser millimeter wave massive MIMO systems," *IEEE Trans. Wireless Commun.*, vol. 18, no. 2, pp. 1041–1053, Feb. 2019.

[9] K. Chen, C. Qi, and G. Y. Li, "Two-step codeword design for millimeter wave massive MIMO systems with quantized phase shifters," *IEEE Trans. Signal Process.*, vol. 68, pp. 170–180, 2020.

[10] S.-E. Chiu, N. Ronquillo, and T. Javidi, "Active learning and CSI acquisition for mmWave initial alignment," *IEEE J. Sel. Areas Commun.*, vol. 37, no. 11, pp. 2474–2489, Nov. 2019.